Desalination and Water Treatment
www.deswater.com

doi: 10.5004/dwt.2023.29955

310 (2023) 68–77
October

Enhancing desalination rate and water recovery through operational optimization of a membrane capacitive deionization system

Dong-Hyun Lee, Jae-Hwan Choi*

Department of Chemical Engineering, Center for Future Sustainable Technology, Kongju National University, 1223-24 Cheonan-daero, Seobuk-gu, Cheonan-si, Chungnam-do, 31080, South Korea, Tel.: +82-41-521-9362; Fax. +82-41-521-9353; emails: jhchoi@kongju.ac.kr (J.-H. Choi), lcslmh2@naver.com (D.-H. Lee)

Received 29 June 2023; Accepted 7 September 2023

ABSTRACT

In this study, the operating conditions of a membrane capacitive deionization (MCDI) system were optimized to enhance the desalination rate and water recovery (WR). To improve WR, an intermittent flow mode (IFM) was implemented in the system; the mode comprised a pause step (solution supply interruption) and flush step (solution supply resumption), during desorption. Optimal desorption conditions were determined through desorption experiments by considering pause time (PT) and flush time (FT). Additionally, adsorption was conducted at various current densities by controlling the total adsorption charge below the maximum allowable charge (MAC). The desorption rate (discharge rate) exhibited no significant difference when desorption was performed with or without solution supply to the MCDI cell. Analysis of the discharge rate during the pause step indicated that it was desirable to set the PT to discharge approximately 90% of the total charge accumulated in the carbon electrode. Furthermore, as FT decreased, WR increased, and the residual charge on the carbon electrode increased. Consequently, during adsorption, the cell potential increased, leading to electrode reactions. On the other hand, by increasing the current density while keeping the supplied charge to the cell below the MAC value, it was confirmed that electrode reactions did not occur, even at a cell potential of approximately 3.0 V. Increasing the current density correspondingly increased the desalination rate and salt removal efficiency, but it decreased WR.

Keywords: Membrane capacitive deionization; Intermittent flow mode; Water recovery, Desalination rate; Maximum allowable charge

1. Introduction

Capacitive deionization (CDI) is an electrochemical deionization technology that involves removing ions from aqueous solutions using a pair of porous carbon electrodes. CDI operates on the principle that ions with opposite charges are adsorbed onto the surfaces of charged electrodes through electrostatic attraction. CDI is recognized as an environmentally friendly technology due to its low level of energy consumption and lack of pollutant generation during desalination [1–5]. Due to these advantages, CDI is gaining significant attention as a future desalination technology.

Typically, a CDI cell comprises a pair of carbon electrodes that are separated by a spacer. The adsorption and desorption processes are performed by adjusting the cell potential while supplying brine through the spacer. After applying a potential to the cell, ions in the feed stream are adsorbed onto a charged electrode. Once the carbon electrode reaches saturation, the adsorbed ions are desorbed into the feed stream by either shorting the electrodes or applying a reverse potential [1,2]. In the conventional CDI cell structure, continuous desalination is not achievable, as the adsorption and desorption processes are repeated within a single feed stream. To overcome this limitation,

* Corresponding author.

flow–electrode CDI (FCDI), which is capable of continuous desalination, has been introduced [6]. Moreover, various CDI cell structures have been developed, including inverted CDI (i-CDI), hybrid CDI, and flow-through CDI [2,7–10]. However, most CDI-related studies (approximately 85%) are based on conventional CDI (flow-by CDI) or membrane capacitive deionization (MCDI), wherein adsorption and desorption occur in a single feed stream [10].

As interest in CDI has increased over the past 20 y, there has been an exponential growth in the number of published research papers. However, most scholars have focused on electrode development (54.5%) and applications (19.6%) [11]. Various carbon electrodes have been developed using carbon-based materials, such as activated carbon, carbon nanotubes, graphene, and carbon aerogels [12–15]. The morphologies and structures of the electrodes, including their pore size distribution, and surface functionalization characteristics, have been optimized [16–18]. Additionally, hybrid electrodes that combine carbon with certain materials, such as metal oxides or functional polymers, have been developed [19–23]. Therefore, the adsorption performance levels of carbon electrodes for CDI have improved significantly. To facilitate the commercialization of the CDI process, it is essential to study carbon electrodes with excellent performance levels and ensure the efficient operation of the system. However, research remains scarce on operational technologies aimed at enhancing the stability and efficiency of the CDI system.

The desalination performance of the CDI system is assessed using various indicators. Representative indicators include the salt adsorption capacity (SAC), charge efficiency (CE), average salt adsorption rate (ASAR), water recovery (WR), salt removal efficiency (SRE), and specific energy consumption (SEC) [2,24–30]. Among these indicators, SAC and CE are primarily influenced by the carbon electrode and cell structure. SAC serves as an indicator of the adsorption capacities of carbon electrodes. CE, which represents the ratio of the charge supplied to the electrode and the adsorbed salt, has significantly improved with the introduction of the MCDI cell structure, which combines an ion exchange membrane and a carbon electrode [31]. On the other hand, the ASAR, WR, SRE, and SEC exhibit notable variations depending on the operating conditions of the CDI system. The ASAR is calculated by dividing the mass of the adsorbed salt by the cycle time (CT), which is the sum of the adsorption time (AT), and the desorption time (DT) [2]. Therefore, reducing CT as much as possible is essential to increasing the ASAR. WR refers to the volume ratio of demineralized water to the total volume of influent supplied to the cell [29,30]. To enhance WR, minimizing the volume of discharged water during desorption is necessary.

During the adsorption and desorption processes of the CDI system, the desalted and concentrated solutions are discharged separately. Fig. 1 shows illustrations of the two operating modes of the CDI system based on the influent supply method during desorption. The continuous flow mode (CFM) involves continuously supplying influent throughout desorption. In this case, as the DT increases, the volume of discharged water (V_{de}) increases, thus decreasing WR. To enhance WR, the desorption process can be performed in intermittent flow mode (IFM). The IFM desorption process consists of pauses and flush steps. During the pause step, desorption (discharge) occurs while the solution supply is temporarily stopped. Since no solution is supplied, the ions desorbed from the carbon electrode become concentrated in the feed stream inside the cell. The accumulated salt is then discharged during the flush step, where solution is supplied. The volume of discharged water in the IFM is determined by the flush time. Therefore, compared with CFM, IFM can increase WR by reducing the volume of discharged water.

To increase the ASAR in the CDI process, it is necessary to reduce the AT. AT can be minimized by increasing the cell

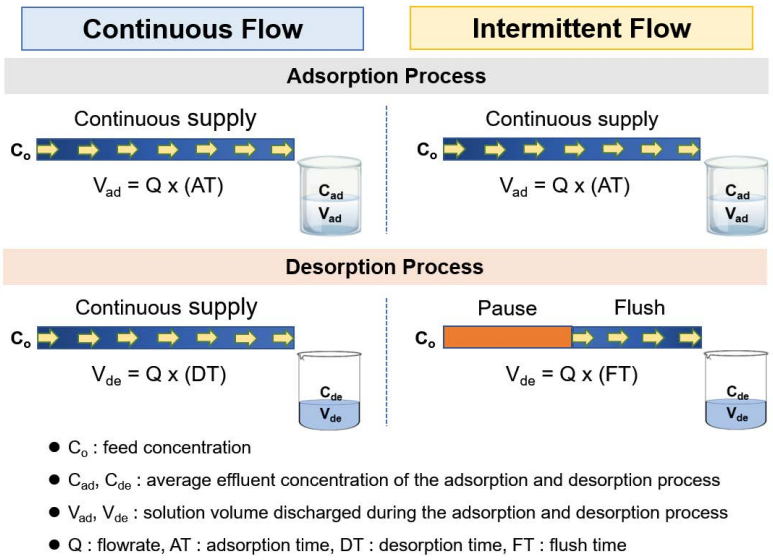

Fig. 1. Solution supply methods in capacitive deionization system operation. (a) Continuous flow mode, where the solution is continuously supplied during desorption. (b) Intermittent flow mode, with pause and flush steps during desorption, where the solution supply is stopped in the pause step and the desorbed ions are discharged by supplying the solution in the flush step.

potential or current density during adsorption. However, if the cell potential is not properly regulated, Faradaic reactions can occur at the carbon electrode, significantly impacting the stability and desalination performance characteristics of the CDI system [32–34]. To ensure stable operation of the MCDI system, irrespective of the cell potential, a new operational approach based on the maximum allowable charge (MAC) was introduced. Yoon and Choi [35] defined MAC as the total charge accumulated on the carbon electrode at the onset of electrode reactions. By controlling the total charge supplied to the carbon electrode below the MAC value, electrode reactions can be prevented, regardless of the cell potential [36–38]. Applying the MAC concept allows flexible control of the cell potential and current density during adsorption. Consequently, AT can be significantly reduced, thus improving ASAR.

The aim of this study is to determine the optimal operating conditions for increasing the desalination rate and WR of the MCDI system. To achieve this objective, the desalination performance of the MCDI system was analyzed, including SAC, CE, ASAR, WR, SRE, and SEC, under various operating conditions. The desorption characteristics are examined based on the influent supply methods (CFM and IFM) using the MCDI unit cell. Furthermore, the optimal pause time (PT) and flush time (FT) are derived by evaluating the desalination performance while varying these parameters in the IFM. Additionally, the effect of the current density on the desalination performance of the MCDI system is analyzed during adsorption.

2. Experiment setup

2.1. Experimental setup for MCDI experiments

An MCDI unit cell was constructed using a commercially available carbon electrode obtained from PuriChem Co., Korea. The carbon electrode was cut into a diameter of 10.5 cm (effective area = 85 cm^2, mass of carbon layer = 1.22 g) using a circular specimen cutter. A 1-cm-diameter hole was drilled in the center of the carbon electrode to allow for effluent discharge. The ion exchange membrane was cut to match the size of the carbon electrode. An anion exchange membrane (ASE, Astom Co., Japan) was positioned on the anode carbon electrode, while a cation exchange membrane (CSE, Astom Co., Japan) was placed on the cathode carbon electrode. To allow the influent to pass, a spacer (EX31-071/80 PW, NBC Meshtec Inc., Japan) with a thickness of 180 μm was inserted between the ion-exchange membranes. The influent was introduced from the outer side of the circular carbon electrode, passed through the spacer, and exited through the central hole.

The MCDI experiments were conducted using a NaCl solution with a concentration of 585 mg/L. The influent was supplied to the MCDI cell at a flow rate of 40 mL/min using a peristaltic pump. The potential and current applied to the cell during adsorption and desorption were controlled using a potentiostat (WPG100, WonA Tech Co., Korea). Additionally, conductivity (Con-BTA) and pH (pH-BTA; Vernier Software & Technology, USA) sensors were installed at the effluent discharge point. The measurements of conductivity and pH were performed through an interface connected to a computer. The configuration of the MCDI cell and the experimental setup of the MCDI system are illustrated in Fig. S1.

2.2. Operation of the MCDI system in continuous and intermittent flow modes

The desorption characteristics were compared based on the solution supply method (CFM and IFM). Prior to desorption, adsorption was conducted for 240 s while applying a current density of 2.35 mA/cm^2 to the cell. After completing adsorption, the cell potential was switched to −0.1 V, and desorption lasted for 600 s. The desorption process was performed in CFM and IFM. In CFM, the solution was continuously supplied to the cell throughout a DT of 600 s. Conversely, in the IFM, the solution supply was paused for the first 420 s and then resumed for 180 s.

To establish a dynamic steady state for the MCDI system, the adsorption–desorption cycle was repeated 10 times for each operation condition. Additionally, the desalination experiment was replicated twice under the same conditions to verify the reproducibility of the desalination performance. During the desalination experiment, the potential, current, and charge that were supplied to the cell and the conductivity and pH of the effluent were automatically measured at 2-s intervals. A correlation between the concentration and the conductivity of the NaCl solution was established for the conductivity sensor. By using this correlation equation, the NaCl concentration was calculated from the conductivity of the effluent.

2.3. MCDI experiments at various operational parameters

Operating the desorption process in IFM could be more effective than CFM for increasing WR. To determine the optimal conditions for IFM, the desalination characteristics were analyzed by varying the PT and FT. After conducting adsorption for 240 s at a current density of 2.35 mA/cm^2, desorption was performed by switching the cell potential to −0.10 V. The desorption characteristics were evaluated by varying PT and FT.

First, to analyze the desorption characteristics with respect to PT, the desorption process was conducted with PT ranging from 120 to 420 s while fixing FT at 180 s. Then, with PT fixed at 180 s, desalination was performed while changing FT from 30 to 180 s, and the desalination characteristics were analyzed based on FT.

The MCDI experiments were performed at different current densities to assess the desalination performance. The current density was adjusted from 2.35 to 5.88 mA/cm^2. According to a previous study, the MAC value of the carbon electrode used in the experiment was 45.3 C/g [39]. Based on this finding, adsorption was conducted until the total charge supplied to the carbon electrode reached 39.3 C/g (86.8% of the MAC value) for each current density. After adsorption, desorption was performed for 226 s at a cell potential of −0.10 V. The desorption was performed in IFM with a PT of 180 s and an FT of 46 s.

The adsorption–desorption cycles were repeated 10 times for each operating condition. Furthermore, the MCDI experiment was conducted twice under the same conditions to ensure the reproducibility of the results. Throughout the

experiment, various measurements were taken, including the potential, current, and charge applied to the cell and the concentration and pH of the effluent. Based on these measurements, the desalination performances (SAC, CE, WR, ASAR, SRE, and SEC) were evaluated using the equations provided below [2,29].

$$\mathrm{SAC}\left(\mathrm{mg/g}\right)=\frac{\left(C_0-C_{\mathrm{avg}}\right)\cdot V_{\mathrm{ad}}}{m} \tag{1}$$

$$\mathrm{CE}\left(\%\right)=\frac{\left(C_0-C_{\mathrm{avg}}\right)\cdot V_{\mathrm{ad}}\cdot F}{M_{\mathrm{NaCl}}\cdot I\cdot\left(\mathrm{AT}\right)}\times 100 \tag{2}$$

$$\mathrm{SRE}\left(\%\right)=\frac{\left(C_0-C_{\mathrm{avg}}\right)}{\left(C_0\right)}\times 100 \tag{3}$$

$$\mathrm{ASAR}\left(\mathrm{mg/g\cdot m}\right)=\frac{\mathrm{SAC}}{\left(\mathrm{AT}+\mathrm{DT}\right)}=\frac{\mathrm{SAC}}{\mathrm{CT}} \tag{4}$$

$$\mathrm{WR}\left(\%\right)=\frac{Q\cdot\left(\mathrm{FT}\right)}{Q\cdot\left(\mathrm{AT}+\mathrm{FT}\right)}\times 100=\frac{\mathrm{FT}}{\left(\mathrm{AT}+\mathrm{FT}\right)}\times 100 \tag{5}$$

$$\mathrm{SEC}\left(\mathrm{J/gNaCl}\right)=\frac{\int_{\mathrm{ad}} I\cdot\Phi dt}{\left(C_o-C_{\mathrm{avg}}\right)\cdot V_{\mathrm{ad}}} \tag{6}$$

where C_0 is the influent concentration (mg/L), C_{avg} and V_{ad} are the average concentration (mg/L) and total volume (L) of the effluent during adsorption, m is the mass of the carbon electrode (g), M_{NaCl} is the molar mass of NaCl (mg/mol), I is the current supplied to the cell during adsorption (A), F is the Faraday constant (96,485 C/mol), Q is the influent flow rate (mL/min), and Φ is the cell potential.

3. Results and discussion

3.1. Desorption characteristics of MCDI cells depending on the solution supply method

After conducting adsorption for 240 s at a constant current of 2.35 mA/cm², desorption was performed for 600 s with a cell potential of −0.10 V. Fig. 2a shows the change in effluent concentration during desorption in the CFM and IFM. In the CFM, where the solution was continuously supplied, rapid desorption occurred initially, resulting in the effluent concentration reaching a maximum value of 1,420 mg/L. Subsequently, the effluent concentration gradually decreased and eventually approached the influent concentration of 585 mg/L. In contrast, during the pause step (420 s) of IFM, the solution supply was halted, allowing the desorbed ions to accumulate in the feed stream inside the cell. When the solution was reintroduced in the flush step, the concentrated salt was discharged completely, thus significantly increasing the effluent concentration. Consequently, the maximum effluent concentration in the IFM reached 4,290 mg/L, which is approximately three times higher than that in the CFM. Furthermore, approximately 60 s after the introduction of the flush solution, the effluent concentration converged to the influent concentration.

The transport rate and mass of ions transported during the MCDI operation could be analyzed based on the current density and cumulative charge supplied to the cell [35]. Fig. 2b depicts the changes in current density and cumulative desorption charge over time during desorption. Evidently, desorption progressed rapidly after applying the desorption potential, regardless of the solution supply method. This phenomenon indicated that ions were efficiently desorbed and moved to the feed stream due to the high electrode potential, even without solution supply. As ions were desorbed, the electrode potential decreased, thus exponentially decreasing the current density. Additionally, a slight increase in current density was observed when the solution was supplied during the IFM flush step.

Regardless of the solution supply method, the total desorption charge during desorption was 39.3 C/g, which is the same as the charge supplied during adsorption. This finding demonstrated that the charge supplied during adsorption was completely discharged during desorption. In CFM, the desorption charge at 420 s was 39.0 C/g (99.0% of the total desorption charge). Similarly, the desorption charge during the pause step (420 s) of IFM was 37.4 C/g, showing no significant difference from CFM. Thus, it was inferred that the discharge rate (desorption rate) was not greatly influenced by the solution supply method.

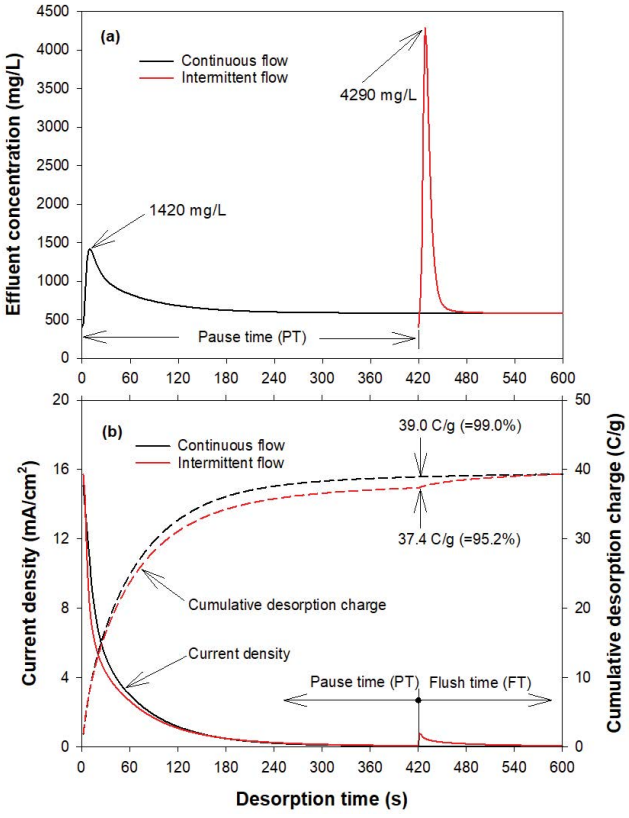

Fig. 2. Changes in (a) effluent concentration and (b) current density during desorption at different solution supply methods. Desorption processes were performed after the adsorption process at a current density of 2.35 mA/cm² for 240 s.

WR in the MCDI process was determined by the volume of effluent during desorption. To enhance WR, it is essential to minimize the volume of the desorption solution. The desorption process in CFM increased the discharged water volume, potentially reducing WR. However, IFM was advantageous for increasing WR because the solution was discharged during the flush step. Therefore, WR could be significantly enhanced by optimizing the PT and FT in the IFM.

3.2. Effect of the pause time in the intermittent flow mode

The optimal PT was determined by analyzing the desorption characteristics in IFM with varying PT's. After completing the adsorption process (240 s @ 2.35 mA/cm^2), the desorption process was performed while changing PT from 120 to 420 s, with FT fixed at 180 s. Fig. 3 shows the concentration change in the effluent during desorption at different PTs. During the pause step, ions desorbed from the electrodes accumulated in the feed stream inside the cell. When the solution was supplied, the concentrated salt was discharged at once, thus rapidly increasing the effluent concentration. As PT increased, the desorption charge was expected to increase, thus increasing the concentration of salt in the feed stream. Consequently, as PT increased from 120 to 420 s, the maximum effluent concentration increased from 4,180 to 4,640 mg/L. In the IFM, the DT was the sum of the PT and FT. Since the solution was supplied during the flush step, FT played a crucial role in determining WR. Thus, it was desirable to minimize FT. If the PT was overly short, a long FT was required for complete discharge. Therefore, to reduce FT, it was recommended to set the PT in a manner that allowed the desorption of most ions during the pause step.

To determine the optimal PT, the cumulative desorption charge over time was analyzed during desorption. Fig. 4 shows the changes in the cumulative charge during the pause and flush steps when PT was varied. The inset in Fig. 4 displays the total desorption charge at the pause and flush steps. Regardless of the PT, the discharge rates during the pause step were evidently similar. As PT increased from 120 to 420 s, the desorption charge in the pause step increased from 31.0 to 37.4 C/g. Conversely, the desorption charge in the flush step decreased from 8.3 to 2.0 C/g as PT increased. The cumulative desorption charges in both the pause and flush steps amounted to 39.3 C/g, which is identical to the charge supplied during adsorption.

As the PT was shortened, the total desorption charge during the pause step decreased. Consequently, a relatively long FT could be necessary to discharge all the accumulated charges on the carbon electrode. Conversely, if the PT was increased, the FT could be reduced, potentially increasing the DT. Therefore, it was necessary to determine the optimal PT by considering the discharge rate during the pause step. Fig. 4 shows that the cumulative desorption charge increased rapidly until approximately 180 s after the start of desorption. At PT = 180 s, the cumulative desorption charge reached 35.1 C/g. This finding indicated that the discharge proceeded rapidly until approximately 90% of the charge accumulated on the carbon electrode was discharged, after which the discharge rate gradually declined. Therefore, the most efficient approach was to discharge approximately 90% of the total desorption charge during the pause step and to discharge the remaining amount during the flush step. Based on this analysis, the optimal PT was 180 s.

3.3. Determination of optimal flush time in the intermittent flow mode

After conducting adsorption for 240 s at a current density of 2.35 mA/cm^2, desorption was performed with a fixed PT of 180 s and an FT that varied from 30 to 180 s. Fig. 5 shows the total desorption charge in the pause and flush steps as FT was changed. The sum of the desorption charges in the pause and flush steps was 39.3 C/g, indicating that all the charges supplied during adsorption were discharged during desorption. However, as the FT was shortened, the

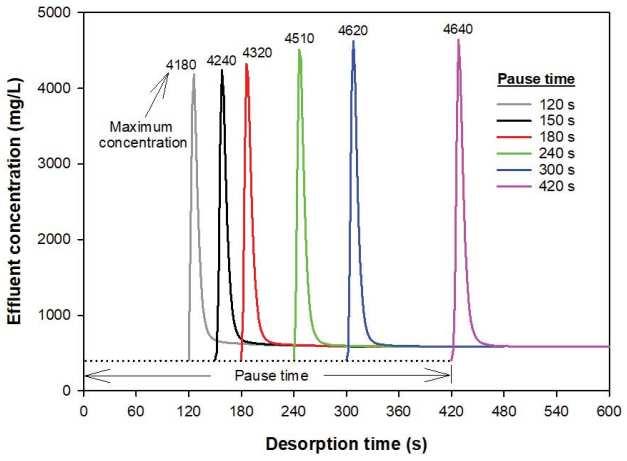

Fig. 3. Changes in effluent concentration during desorption at various pause times. Desorption processes were performed after the adsorption process at a current density of 2.35 mA/cm^2 for 240 s.

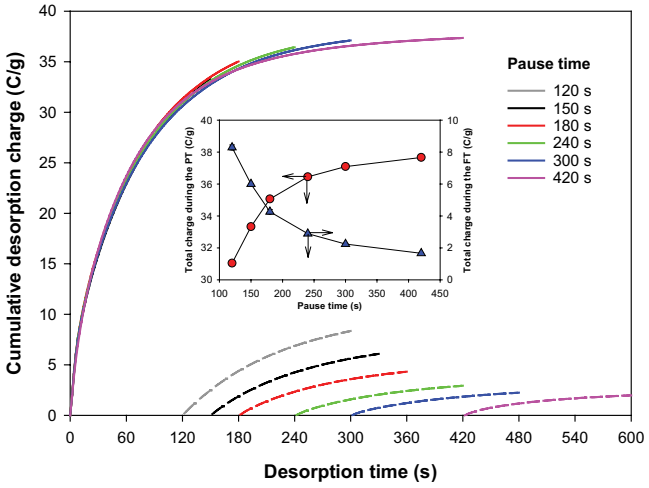

Fig. 4. Cumulative desorption charges at different pause times. The solid and dotted lines represent the cumulative desorption charge in the pause and flush steps, respectively. The inset shows the total desorption charge during the pause and flush times.

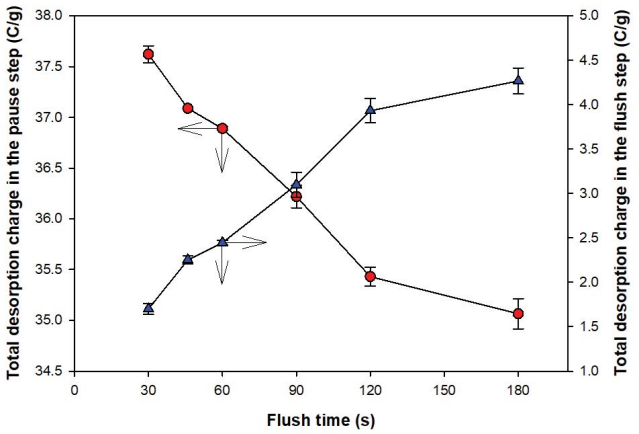

Fig. 5. Variations in total desorption charges during the pause and flush times. Desorption processes were performed with a fixed PT of 180 s and varying FT from 30 to 180 s.

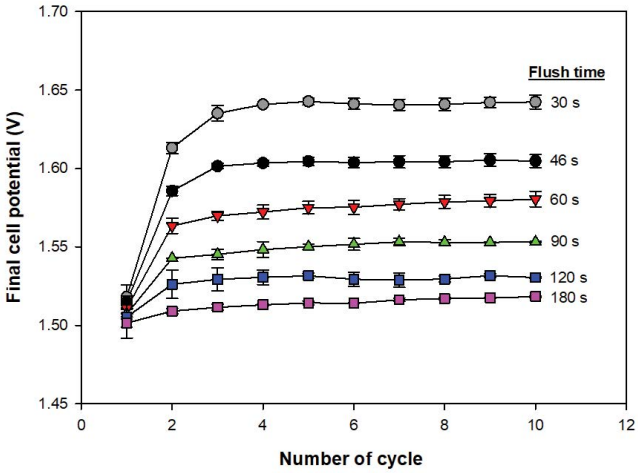

Fig. 6. Changes in the final cell potential during adsorption according to the number of cycles. The adsorption process was conducted at a current density of 2.35 mA/cm^2 for 240 s, while the desorption process was performed with a fixed PT of 180 s and varying FT from 30 to 180 s.

desorption charge in the pause step increased, while the desorption charge in the flush step decreased. At FTs of 180 and 30 s, the desorption charges during the pause step were 35.1 and 37.6 C/g, respectively. The number of desorbed ions was expected to increase as the desorption charge in the pause step increased. In fact, measuring the effluent concentration during the flush step (Fig. S2), confirmed that the maximum concentration of the effluent increased as the FT decreased.

The charges that remained undischarged during the pause step were subsequently discharged in the flush step. Sufficient time was required for complete discharge during the flush step. If the FT was insufficiently long, some charges remained on the carbon electrode. Moreover, as the FT decreased, the amount of residual charge (Q_{re}) increased. When the adsorption process was repeated with an adsorption charge (Q_{ad}) of 39.3 C/g while the charge remained on the carbon electrode, the total charge accumulated on the carbon electrode ($Q_T = Q_{re} + Q_{ad}$) increased. Since Q_{re} increased as FT decreased, the Q_T of the carbon electrode increased upon completion of the adsorption process. In a previous study, it was observed that the discharge rate during desorption was proportional to Q_T [39]. Consequently, as the FT decreased, the Q_T of the carbon electrode increased, thus increasing the desorption charge during the pause step.

Fig. 6 displays the final cell potential measured during the adsorption of each cycle, with the adsorption–desorption cycle repeated 10 times. For all FTs, the cell potential in the first cycle exhibited similar values ranging from 1.50 to 1.52 V. However, as the cycles were repeated, the cell potential increased until the third cycle and then stabilized. Moreover, a significant increase in the final cell potential was observed as the FT shortened. For FT = 180 s, the final cell potentials in the first and tenth cycles were 1.50 and 1.52 V, respectively, with no significant difference. However, for FT = 30 s, the cell potential increased by 0.12 V from 1.52 to 1.64 V. Since the electrode potential was directly related to the charge stored in the carbon electrode, the cell potential increased as Q_T increased [35,39]. As mentioned previously, as FT decreased, Q_{re} increased, thus increasing Q_T. Consequently, it was inferred that the cell potential gradually increased with decreasing FT.

Fig. S3 depicts the pH change in the effluent during the repeated adsorption–desorption cycle with varying FTs. When the FT was greater than 46 s, the pH of the effluent remained stable throughout the cycle repetitions. However, at FT = 30 s, the pH gradually decreased as the cycle was repeated. The pH change in the effluent during MCDI operation was attributed to electrode reactions [40]. When FT was shortened, the Q_T of the carbon electrode increased during adsorption due to the accumulation of Q_{re}. Once Q_T surpasses the MAC value of the carbon electrode (45.3 C/g), an electrode reaction occurs. Based on Fig. S3, it was inferred that electrode reactions did not occur until the FT was 46 s. However, at FT = 30 s, the Q_T of the carbon electrode exceeded the MAC value due to Q_{re}, indicating the occurrence of electrode reactions. Electrode reactions during MCDI operation could pose significant challenges to desalination performance and system stability [34]. Therefore, the optimal FT, which could enhance WR while ensuring stability against electrode reactions, was 46 s.

3.4. Desalination performance with the current density of the adsorption process

Increasing the current density applied to the cell during adsorption could shorten the AT and increase the ASAR. Adsorption was conducted by varying the current density from 2.35 to 5.88 mA/cm^2 until a total charge of 39.3 C/g was applied to the cell. The desorption process was performed under the optimized desorption conditions (PT = 180 s, FT = 46 s, and DT = 226 s). Fig. 7 shows the changes in effluent concentration and cell potential during adsorption at different current densities. As the current was applied, the concentration of the effluent first rapidly decreased and then reached a constant state. With increasing current density, the AT was shortened from 240 to 96 s, and the effluent concentration decreased from 405 to 143 mg/L.

Table 1
Desalination performance levels of MCDI experiments at different current densities

Current density (mA/cm^2)	SAC (mg/g)	CE (%)	SRE (%)	ASAR (mg/g·min)	WR (%)	SEC (kJ/g)
2.35	11.61 ± 0.04	97.4 ± 0.3	30.3 ± 0.1	1.50 ± 0.01	83.9	2.01 ± 0.00
3.53	11.52 ± 0.01	96.6 ± 0.1	45.0 ± 0.0	1.79 ± 0.00	77.7	2.51 ± 0.01
4.71	11.43 ± 0.03	95.9 ± 0.2	59.6 ± 0.1	1.98 ± 0.01	72.3	3.05 ± 0.04
5.88	10.97 ± 0.02	92.0 ± 0.1	71.5 ± 0.1	2.04 ± 0.00	67.6	4.85 ± 0.13

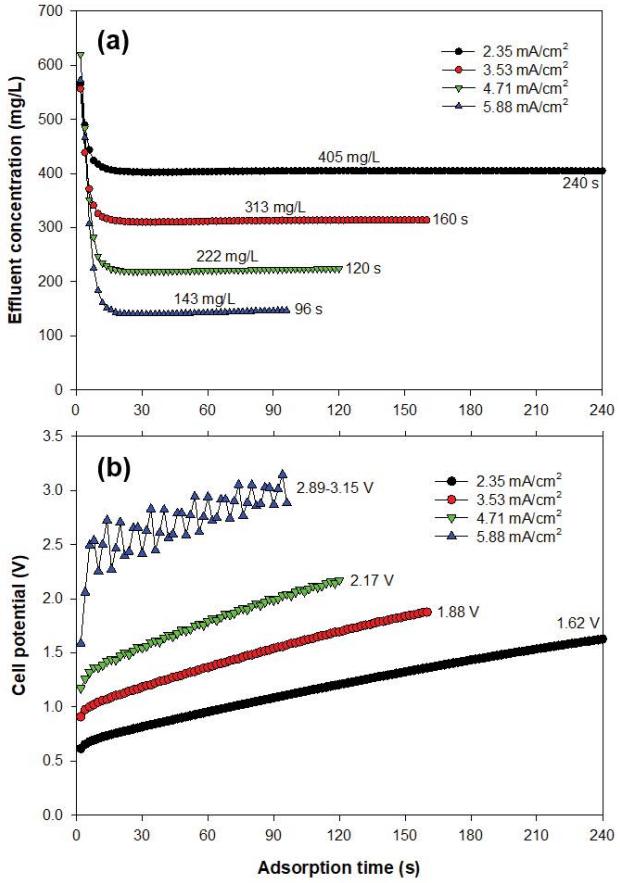

Fig. 7. Changes in (a) effluent concentration and (b) cell potential during adsorption at various current densities. The desorption process was performed for 226 s at a cell potential of −0.10 V, with a PT of 180 s and an FT of 46 s.

Conversely, as the charge accumulated on the carbon electrode increased, the cell potential exhibited a linear increase over time. Additionally, the cell potential increased with increasing current densities. This relationship between cell potential and current density was attributed to the decrease in feed stream concentration and the consequent increase in electrical resistance. Consequently, it was inferred that the iR drop in the feed stream intensified, thus increasing the cell potential. Notably, at a current density of 5.88 mA/cm^2, the cell potential displayed fluctuations. This behavior could be attributed to concentration variations in the feed stream caused by the pulsation phenomenon during influent water supply via a peristaltic pump. By altering the current density from 2.35 to 5.88 mA/cm^2, the final cell potential increased from 1.62 V to a maximum value of 3.15 V. However, as depicted in Fig. S4, the pH of the effluent remained stable during ten cycles of adsorption–desorption at a current density of 5.88 mA/cm^2. This observation confirmed that the electrode reaction did not occur, even at cell potentials of 3 V or higher, as long as the charge supplied during adsorption was controlled to be below the MAC value.

The desalination performance indicators (SAC, CE, SRE, ASAR, WR, and SEC) for MCDI experiments at varying current densities were calculated and are presented in Table 1.

As the current density increased, a slight decrease was observed in SAC and CE. This decrease could be attributed to the shortened AT value at high current densities. The initial effluent concentration during adsorption could influence the average concentration of the effluent. Conversely, as the current density increased, the effluent concentration decreased, and the SRE increased proportionally. Additionally, the shortened AT increased the desalination rate, ASAR, by 36%, from 1.50 to 2.04 mg/g·min. However, the increased current density decreased the volume of desalted water, thus decreasing WR. Furthermore, there was a significant increase in SEC due to the increased electrical resistance. Table 1 clearly demonstrates the significant variation in the desalination performance of the MCDI system depending on the current density. Additionally, the desalination performance indicators exhibited conflicting relationships with each other. Therefore, it was essential to consider the purpose of desalination when determining the optimal operating conditions for the MCDI system.

4. Conclusion

Optimal operating conditions were determined to enhance the desalination performance of an MCDI system. The desorption characteristics were analyzed based on the influent supply method. Desorption experiments were conducted to derive the optimal desorption conditions by varying the PT and FT in the IFM. Furthermore, MCDI experiments were performed with varying current densities during adsorption, and the desalination performances (SAC, CE, SRE, ASAR, WR, and SEC) were compared. The results revealed that the supply method of the solution did not significantly affect the desorption characteristics. Therefore, it was concluded that operating the desorption process in the IFM mode would be effective to increase WR. Additionally, by considering discharge rates, it was recommended to set the PT so that approximately 90% of the total desorption charge was discharged during the pause

step. On the other hand, as FT decreased, WR increased. This increased the residual charge on the carbon electrode and subsequently increased the cell potential, resulting in electrode reactions. By adjusting the adsorption rate through the current density, significant differences were observed in various desalination performance indicators, such as SRE, ASAR, WR, and SEC.

The desalination performance of the MCDI system can vary depending on specific factors, such as the concentration and composition of the influent, as well as the operating conditions. Additionally, the adsorption capacity and specifications (size and thickness) of the carbon electrode used in the MCDI system can impact the overall desalination performance. WR in the MCDI system is significantly influenced by the desorption rate. To enhance both WR and ASAR, it is crucial to increase the desorption rate. The findings presented in this study are expected to offer valuable insights for optimizing the operating conditions and effectively configuring the MCDI system to meet specific desalination goals.

Acknowledgement

This work was supported by the National Research Foundation of Korea (NRF) grant funded by the Korea government (Ministry of Science and ICT) (NRF-2021R1A2C1003431), and by the research grant of the Kongju National University in 2023.

List of abbreviations

ASAR	—	Average salt adsorption rate
AT	—	Adsorption time
CE	—	Charge efficiency
CFM	—	Continuous flow mode
DT	—	Desorption time
FT	—	Flush time
IFM	—	Intermittent flow mode
PT	—	Pause time
SAC	—	Salt adsorption capacity
SEC	—	Specific energy consumption
SRE	—	Salt removal efficiency
WR	—	Water recovery

References

[1] S. Porada, R. Zhao, A. van der Wal, V. Presser, P.M. Biesheuvel, Review on the science and technology of water desalination by capacitive deionization, Prog. Mater. Sci., 58 (2013) 1388–1442.
[2] M.E. Suss, S. Porada, X. Sun, P.M. Biesheuvel, J. Yoon, V. Presser, Water desalination via capacitive deionization: what is it and what can we expect from it?, Energy Environ. Sci., 8 (2015) 2296–2319.
[3] M.A. Ahmed, S. Tewari, Capacitive deionization: processes, materials and state of the technology, J. Electroanal. Chem., 813 (2018) 178–192.
[4] J. Landon, X. Gao, A. Omosebi, K. Liu, Progress and outlook for capacitive deionization technology, Curr. Opin. Chem. Eng., 25 (2019) 1–8.
[5] S.D. Datar, R. Mane, N. Jha, Recent progress in materials and architectures for capacitive deionization: a comprehensive review, Water Environ. Res., 94 (2022) e10696, doi: 10.1002/wer.10696.
[6] S.I. Jeon, H.R. Park, J.G. Yeo, S. Yang, C.H. Cho, M.H. Han, D.K. Kim, Desalination via a new membrane capacitive deionization process utilizing flow-electrodes, Energy Environ. Sci., 6 (2013) 1471–1475.
[7] F. Yang, Y. He, L. Rosentsvit, M.E. Suss, Z. Zhang, T. Gao, P. Liang, Flow-electrode capacitive deionization: a review and new perspectives, Water Res., 200 (2021) 117222, doi: 10.1016/j.watres.2021.117222.
[8] X. Gao, A. Omosebi, J. Landon, K. Liu, Surface charge enhanced carbon electrodes for stable and efficient capacitive deionization using inverted adsorption–desorption behavior, Energy Environ. Sci., 8 (2015) 897–909.
[9] J. Lee, S. Kim, C. Kim, J. Yoon, Hybrid capacitive deionization to enhance the desalination performance of capacitive deionization, Energy Environ. Sci., 7 (2014) 3683–3689.
[10] W. Tang, J. Liang, D. He. J. Gong, L. Tang, Z. Liu, D. Wang, G. Zeng, Various cell architectures of capacitive deionization: recent advances and future trends, Water Res., 150 (2019) 225–251.
[11] J. Choi, P. Dorji, H.K. Shon, S. Hong, Applications of capacitive deionization: desalination, softening, selective removal, and energy efficiency, Desalination, 449 (2019) 118–130.
[12] Z.H. Huang, Z. Yang, F. Kang, M. Inagaki, Carbon electrodes for capacitive deionization, J. Mater. Chem. A, 5 (2017) 470–496.
[13] Z. Zhao, H. Wei, H. Zhao, Y. Wang, N. Tang, Electrode materials for capacitive deionization: a review, J. Electroanal. Chem., 873 (2020) 114416, doi: 10.1016/j.jelechem.2020.114416.
[14] S. Vafakhah, Z. Beiramzaheh, M. Saeedikhani, H.Y. Yang, A review on free-standing electrodes for energy-effective desalination: recent advances and perspectives in capacitive deionization, Desalination, 49 (2020) 114662, doi: 10.1016/j.desal.2020.114662.
[15] M.A. Luciano, H. Ribeiro, G.E. Bruch, G.G. Silva, Efficiency for capacitive deionization using carbon materials-based electrodes for water desalination, J. Electroanal. Chem., 859 (2020) 113840, doi: 10.1016/j.jelechem.2020.113840.
[16] L. Han, K.G. Karthikeyan, M.A. Anderson, K.B. Gregory, Exploring the impact of pore size distribution on the performance of carbon electrodes for capacitive deionization, J. Colloid Interface Sci., 430 (2014) 93–99.
[17] Y. Cheng, Z. Hao, C. Hao, Y. Deng, X. Li, K. Li, Y. Zhao, A review of modification of carbon electrode material in capacitive deionization, RSC Adv., 9 (2019) 24401–24419.
[18] P. Shui, E. Alhseinat, Quantitative insight into the effect of ions size and electrodes pores on capacitive deionization performance, Electrochim. Acta, 329 (2020) 135176, doi: 10.1016/j.electacta.2019.135176.
[19] J. Oladunni, J.H. Zain, A. Hai, F. Banat, G. Bharath, E. Alhseinat, A comprehensive review on recently developed carbon-based nanocomposites for capacitive deionization: from theory to practice, Sep. Purif. Technol., 207 (2018) 291–320.
[20] K. Singh, S. Porada, H.D. de Gier, P.M. Biesheuvel, L.C.P.M. de Smet, Timeline on the application of intercalation materials in capacitive deionization, Desalination, 455 (2019) 115–134.
[21] R.L. Zornitta, L.A.M. Ruotolo, L.C.P.M. de Smet, High-performance carbon electrodes modified with polyaniline for stable and selective anion separation, Sep. Purif. Technol., 290 (2022) 120807, doi: 10.1016/j.seppur.2022.120807.
[22] X. Xu, M. Eguchi, Y. Asakura, L. Pan, Y. Yamauchi, Metal–organic framework derivatives for promoted capacitive deionization oxygenated saline water, Energy Environ. Sci., 16 (2023) 1815–1820.
[23] X. Liu, X. Xu, X. Xuan, W. Xia, G. Feng, S. Zhang, Z.G. Wu, B. Zhong, X. Guo, K. Xie, Y. Yamauchi, Unlocking enhanced capacitive deionization of $NaTi_2(PO_4)_3$/carbon materials by the yolk-shell design, J. Am. Chem. Soc., 145 (2023) 9242–9253.
[24] R. Zhao, S. Porada, P.M. Biesheuvel, A. van der Wal, Energy consumption in membrane capacitive deionization for different water recoveries and flow rates, and comparison with reverse osmosis, Desalination, 330 (2013) 35–41.
[25] R. Zhao, O. Satpradit, H.H.M. Rijnaarts, P.M. Biesheuvel, A. van der Wal, Optimization of salt adsorption rate in membrane capacitive deionization, Water Res., 47 (2013) 1941–1952.

[26] J. Kang, T. Kim, K. Jo, J. Yoon, Comparison of salt adsorption capacity and energy consumption between constant current and constant voltage operation in capacitive deionization, Desalination, 352 (2014) 52–57.
[27] L. Wang, S. Lin, Intrinsic trade-off between kinetic and energetic efficiencies in membrane capacitive deionization, Water Res., 129 (2018) 394–401.
[28] M.W. Saleem, W.S. Kim, Parameter-based performance evaluation and optimization of a capacitive deionization desalination process, Desalination, 437 (2018) 133–143.
[29] S.A. Hawks, A. Ramachandran, S. Porada, P. Campbel, M.E. Suss, P.M. Biesheuvel, J.G. Santiago, M. Stadermann, Performance metrics for the objective assessment of capacitive deionization systems, Water Res., 152 (2019) 126–137.
[30] A. Ramchandran, D.I. Oyarzun, S.A. Hawks, M. Stadermann, J.G. Santiago, High water recovery and improved thermodynamic efficiency for capacitive deionization using variable flowrate operation, Water Res., 155 (2019) 76–85.
[31] J.B. Lee, K.K. Park, H.M. Eum, C.W. Lee, Desalination of a thermal power plant wastewater by membrane capacitive deionization, Desalination, 196 (2006) 125–134.
[32] D. He, C.E. Wong, W. Tang, P. Kovalsky, T.D. Waite, Faradaic reactions in water desalination by batch-mode capacitive deionization, Environ. Sci. Technol. Lett., 3 (2016) 222–226.
[33] W. Tang, D. He, C. Zhang, P. Kovalsky, T.D. Waite, Comparison of Faradaic reactions in capacitive deionization (CDI) and membrane capacitive deionization (MCDI) water treatment processes, Water Res., 120 (2017) 229–237.
[34] C. Zhang, D. He, J. Ma, W. Tang, T.D. Waite, Faradaic reactions in capacitive deionization (CDI)—problems and possibilities: a review, Water Res., 128 (2018) 314–330.
[35] D.J. Yoon, J.H. Choi, A new standard metric describing the adsorption capacity of carbon electrode used in membrane capacitive deionization, Water Res., 148 (2019) 126–132.
[36] J.H. Choi, D.J. Yoon, A stable operation method for membrane capacitive deionization systems without electrode reactions at high cell potential, Water Res., 157 (2019) 167–174.
[37] J.H. Choi, D.J. Yoon, The maximum allowable charge for operating membrane capacitive deionization without electrode reactions, Sep. Purif. Technol., 215 (2019) 125–133.
[38] J.W. Son, J.H. Choi, Suppression of electrode reactions and enhancement of the desalination performance of capacitive deionization using a composite carbon electrode coated with an ion-exchange polymer, Sep. Purif. Technol., 278 (2021) 119503, doi: 10.1016/j.seppur.2021.119503.
[39] J.W. Son, J.H. Choi, Improvements in desorption rate and electrode stability of membrane capacitive deionization by optimizing operation parameters, Water Res., 220 (2022) 118713, doi: 10.1016/j.watres.2022.118713.
[40] J.E. Dykstra, K.J. Keesman, P.M. Biesheuvel, A. van der Wal, Theory of pH changes in water desalination by capacitive deionization, Water Res., 119 (2017) 178–186.

Supporting information

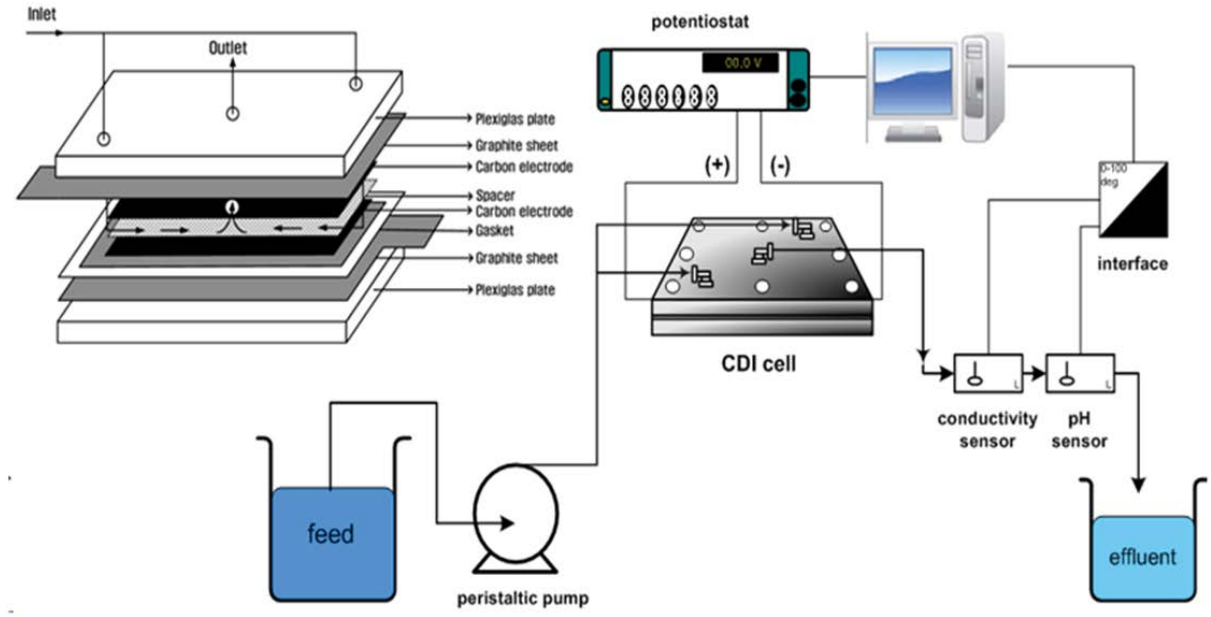

Fig. S1. Configuration of the MCDI cell and the experimental setup of the MCDI system.

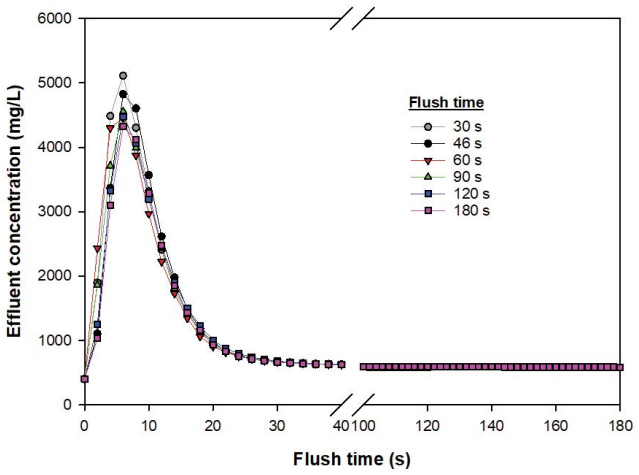

Fig. S2. Changes in effluent concentration during desorption at various flush times. Desorption processes were performed after the adsorption process at a current density of 2.35 mA/cm² for 240 s. The PT was fixed at 180 s, while the FT varied between 30 and 180 s.

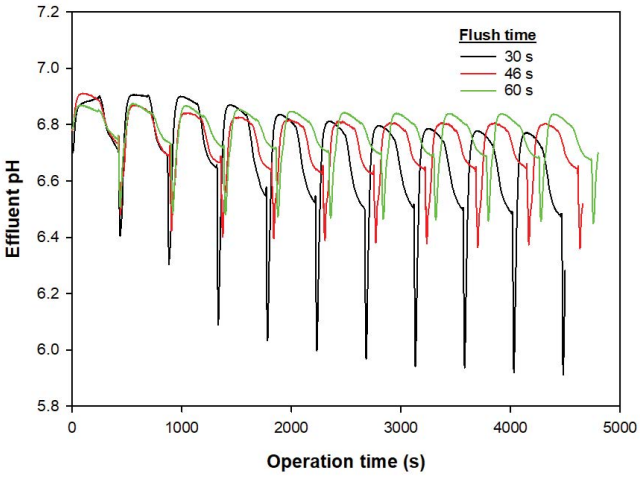

Fig. S3. Changes in effluent pH over ten consecutive cycles of adsorption and desorption processes at flush times of 30, 46, and 60 s. The adsorption process was conducted at a current density of 2.35 mA/cm² for 240 s, while the pause time during desorption was set at 180 s.

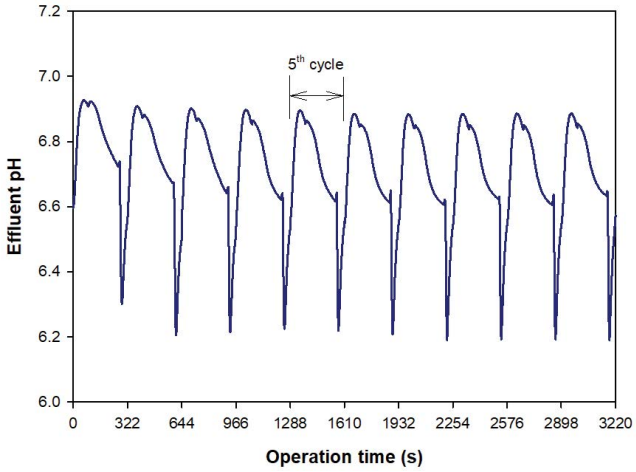

Fig. S4. Changes in effluent pH over ten consecutive cycles of adsorption and desorption. The adsorption process was conducted at a current density of 5.88 mA/cm² for 96 s, and desorption was performed at a cell potential of −0.1 V for 226 s (PT = 180 s and FT = 46 s).